Fungal transformation of natural and synthetic cobalt-bearing manganese oxides and implications for cobalt biogeochemistry

Ferrier, John; Csetenyi, Laszlo; Gadd , Geoffrey Michael

Published in:
Environmental Microbiology

DOI:
10.1111/1462-2920.15526

Publication date:
2021

Document Version
Publisher's PDF, also known as Version of record

environmental microbiology

Environmental Microbiology (2021) **00**(00), 00–00 doi:10.1111/1462-2920.15526

Fungal transformation of natural and synthetic cobalt-bearing manganese oxides and implications for cobalt biogeochemistry

John Ferrier,[1] Laszlo Csetenyi[2] and Geoffrey Michael Gadd [1,3*]

[1]*Geomicrobiology Group, School of Life Sciences, University of Dundee, Dundee, Scotland, DD1 5EH, UK.*
[2]*School of Science and Engineering, Fulton Building, University of Dundee, Dundee, Scotland, DD1 5HN, UK.*
[3]*State Key Laboratory of Heavy Oil Processing, Beijing Key Laboratory of Oil and Gas Pollution Control, College of Chemical Engineering and Environment, China University of Petroleum, 18 Fuxue Road, Changping District, Beijing, 102249, China.*

Summary

Manganese oxide minerals can become enriched in a variety of metals through adsorption and redox processes, and this forms the basis for a close geochemical relationship between Mn oxide phases and Co. Since oxalate-producing fungi can effect geochemical transformation of Mn oxides, an understanding of the fate of Co during such processes could provide new insights on the geochemical behaviour of Co. In this work, the transformation of Mn oxides by *Aspergillus niger* was investigated using a Co-bearing manganiferous laterite, and a synthetic Co-doped birnessite. *A. niger* could transform laterite in both fragmented and powder forms, resulting in formation of biomineral crusts that were composed of Mn oxalates hosting Co, Ni and, in transformed laterite fragments, Mg. Total transformation of Co-doped birnessite resulted in precipitation of Co-bearing Mn oxalate. Fungal transformation of the Mn oxide phases included Mn(III,IV) reduction by oxalate, and may also have involved reduction of Co(III) to Co(II). These findings demonstrate that oxalate-producing fungi can influence Co speciation in Mn oxides, with implications for other hosted metals including Al and Fe. This work also provides further understanding of the roles of fungi as geoactive agents which can inform potential applications in metal bioremediation, recycling and biorecovery.

Introduction

Mn oxides are ubiquitous in terrestrial and aquatic environments and occupy a central role in a range of biogeochemical processes. Mn oxide minerals are extremely redox active and also possess high sorptive capacities, which can lead to considerable enrichment by a range of secondary metals (Post, 1999; Tebo *et al*., 2004). Interactions between microorganisms and Mn oxides have been studied extensively, particularly the precipitation of Mn oxides oxidation of Mn(II) and the reductive dissolution of Mn oxides (Lovley, 1991; Lovley *et al*., 2004; Tebo *et al*., 2004; Miyata *et al*., 2004, 2006a, 2006b). However, less attention has been paid to the fate of the secondary metals that may be associated with the Mn oxide minerals during these processes. In particular, little information exists for cobalt which has a well-established geochemical association with Mn and is commonly hosted in Mn(III,IV) oxide minerals (Manceau *et al*., 1997; Nicholoson and Eley, 1997; Dzemua *et al*., 2013; Kuhn *et al*., 2017). Investigation of the fate of Co during Mn(III,IV) oxide transformations is therefore required to develop a more complete understanding of Co biogeochemistry. Newsome *et al*. (2020) showed that Co mobility in anaerobic laterite sediment microcosms was closely related to Mn release which was primarily attributed to indigenous Mn(IV) and Fe(III) reducing bacteria. This points to a direct relationship between Mn(III,IV) oxide mineral dissolution and Co mobility, and that anaerobic prokaryotes occupy an important role in such processes. However, little information exists on the fate of Co as a result of fungal interactions with Mn oxides, or indeed fungal interactions with Co generally. This is surprising given the capacity of several fungal species to precipitate (e.g. *Acremonium* sp., *Stagonospora* sp. and *Pyrenochaeta* sp.) or solubilize Mn oxides (e.g. *Aspergillus niger*, *Serpula himantioides*), and the

Received 14 January, 2021; revised 8 April, 2021; accepted 12 April, 2021. *For correspondence. Tel: +44 (0) 1382 384767; E-mail g.m.gadd@dundee.ac.uk

common residence of Co within Mn oxide minerals (Post, 1999; Tebo *et al*., 2004; Miyata *et al*., 2004, 2006a, 2006b; Santelli *et al*., 2011; Wei *et al*., 2012; Ferrier *et al*., 2019).

Geoactive fungi play an important role in a range of biogeochemical cycles and their involvement in the dissolution of mineral substrates, as well as in the formation of secondary biomineral phases, is well-established (Gadd 1999, 2007, 2010; Gadd *et al*., 2014). Fungi can mediate the mobilization of nutrients contained within minerals, e.g. phosphate, sulfate, as well as essential, inessential and potentially-toxic metals, e.g. Na, K, Mg, Ca, Mn, Fe, Cu, Zn, Co, Ni, Al, Cs, Cd, Hg, Pb, U) (Burford *et al*., 2003; Fomina *et al*., 2007; Gadd, 2007, 2010; Rhee *et al*., 2012; Ceci *et al*., 2015; Liang *et al*., 2015; Yang *et al*., 2019; Mendes *et al*., 2020). While mineral bioweathering by fungi can be mediated by often synergistic interactions between biophysical and biochemical mechanisms, the secretion of mycogenic organic acids is central to such processes (Gadd, 1999). Oxalic acid secretion is of particular significance and is implicated in the transformation and solubilization of a range of mineral phases including carbonates, phosphates, arsenates, silicates, sulfides and oxides (Sayer and Gadd, 2001; Fomina *et al*., 2004, 2007; Burford *et al*., 2006; Wei *et al*., 2012, 2013; Ceci *et al*., 2015; Ferrier *et al*., 2019; Suyamud *et al*., 2020; Mendes *et al*., 2020). Oxalic acid can attack minerals by both acidolysis and complexolysis (ligand mediated dissolution) as the oxalate anion ($C_2O_4^{2-}$) is a bidentate ligand capable of forming soluble complexes with a range of mono, di, tri and tetravalent cations (Gadd, 1999, 2007, 2010; Gadd *et al*., 2014; Verma *et al*., 2019). In many cases, mineral dissolution and metal release is followed by the precipitation of oxalate biominerals entrapping solubilized metals. Factors that determine soluble complex formation or oxalate precipitation include the valence state of the cation, the relative abundance of oxalate anions and metals in solution, pH and stability constants of the oxalate complexes (Gadd, 1999; Verma *et al*., 2019) For example, simple oxalates containing divalent cations are sparingly soluble or insoluble and readily precipitate over a wide range of pH values (e.g. Ca, Mg, Mn, Co, Ni, Cu) but may also form complexes in the presence of excess oxalate, while trivalent metals such as Al(III) and Fe(III) only exist as soluble complexes (Gadd, 1999; Gadd *et al*., 2014; Verma *et al*., 2019; Kang *et al*, 2019, 2020, 2021; Mendes *et al*., 2020). In addition, oxalate is a reductant which can effect the reduction of some metal species, including Mn(III,IV) to Mn(II), through oxalate precipitation (Wei *et al*., 2012; Verma *et al*., 2019). Oxalic acid has previously been shown to be able to transform natural, biogenic and synthetic Mn oxides. Wei *et al*. (2012) demonstrated the transformation of a biogenic Mn oxide and synthetic birnessite via oxalate secretion by *S. himantioides* and *A. niger*, resulting in Mn(II) oxalate formation via a Mn(III) oxalate intermediate, while Ferrier *et al*. (2019) showed *A. niger* was able to colonize and transform seafloor manganese nodules resulting in Mn and Ca oxalate precipitation.

Mn oxide minerals generally fall into two categories based on the arrangement of edge- or corner-sharing MnO_6 octahedra, the basic structural unit (Post, 1999; Tebo *et al*., 2004). These include phyllomanganates, composed of layers of edge-sharing MnO_6 octahedra (e.g. buserite and birnessite), and tectomanganates, which are composed of chains of edge-sharing MnO_6 octahedra the ends of which share corners with other chains to form tunnel structures (e.g. cryptomelane and todorokite) (Post, 1999; Tebo *et al*., 2004). Due to the presence of vacant octahedral sites, manganates possess large negatively charged surface areas. As a consequence of this, manganates in soils and sediments can incorporate a range of charge-balancing metal cations via adsorption including Ca^{2+}, Co^{2+}, Cu^{2+}, Ni^{2+}, K^{+}, Na^{+} and Mg^{2+} (Post, 1999; Tebo *et al*., 2004). Additionally, surface hydroxyl groups also provide sites for adsorption of metal cations, forming covalent bonds and preventing desorption (Nicholoson and Eley, 1997). In some cases, adsorbed metals are structurally incorporated into the oxides via oxidation and isomorphic substitution. For example, adsorbed Co(II) can be oxidized by layer-residing Mn(III), which then migrates to the interlayer space to be replaced by Co(III) (Manceau *et al*., 1997).

In this work, the fungal transformation of a Co-rich manganiferous laterite from Nkamouna, Cameroon and a synthetic Co-doped birnessite was investigated. The unexploited Nkamouna laterite represents a significant future Co resource, with sufficiently high ore grades to be one of the few operations that can produce Co as the primary metal, with significant quantities of Ni also present (Petavratzi *et al*., 2019). The Mn oxides lithiophorite [$(Al,Li)Mn^{+4}O_2(OH)_2$], asbolane [$(Ni^{2+},Co^{3+})_xMn^{4+}(O,OH)_4{\cdot}nH_2O$] and cryptomelane [$K(Mn^{4+},Mn^{2+})_8O_{16}$] are ore minerals present in the Nkamouna laterite (Dzemua *et al*., 2011, 2013). Lithiophorite is a phyllomanganate composed of alternating stacked layers of MnO_6 and $Al(OH)_6$ octahedra, with $Li(OH)_6$ commonly filling vacant sites in the $Al(OH)_6$ layers, while asbolane is structurally related to lithiophorite but with Al replaced by other transition metals, commonly Ni and Co (Chukhrov *et al*., 1982; Post, 1999). Cryptomelane is part of the hollandite group of tectomanganates, composed of tunnel structures formed by 2×2 chains of MnO_6 octahedra and containing K^{+} as the dominant charge-balancing cation (Post, 1999; Cheney *et al*., 2009). Birnessite ([Na,Ca,Mn(II)]$Mn_7O_{14}{\cdot}2.8H_2O$) is a fine-grained poorly crystalline

phyllomanganate composed of layers of edge-sharing MnO_6 octahedra separated by 7 Å hydrated interlayer spaces (Post, 1999; Tebo *et al*., 2004). Birnessite-type phases are ubiquitous in soils and sediments, and major components of seafloor manganese nodules (Post, 1999; Hein *et al*., 2013). While birnessite is known to occupy a central role in soil redox, sorption and ion-exchange reactions, it can be difficult to isolate due as it is generally present in low quantities and associated with other Mn- and Fe-(oxyhydr)oxides, silicates and/or cell biomass (Toner and Sposito, 2005; Händel *et al*., 2013). Despite this, synthetic birnessites, e.g. K-birnessite, Na-birnessite and acid birnessite can be easily prepared to accommodate geochemical and biogeochemical investigations (Jokic, *et al*., 2001; Tebo *et al*., 2004; Toner and Sposito, 2005; Händel *et al*., 2013; Wang *et al*., 2013). A range of studies have used metal-doped birnessites, including those containing Co, Cu, Al and Ni (Lucht and Medoza-Cortez, 2015; Yadav *et al*., 2017; Arias *et al*., 2019; Legutko *et al*., 2019). In this work, a synthetic Co-doped birnessite was used to provide a general example for the fate of Co during Mn oxide transformations, to complement examination of the Nkamouna laterite. *A. niger* was chosen for this investigation as it can produce substantial quantities of oxalate and has a known capacity to effect manganese oxide transformations (Wei *et al*., 2012; Milová-Žiaková *et al*., 2016; Ferrier *et al*., 2019). It was hypothesised that Co-bearing Mn oxide minerals would be transformed via fungal oxalate secretion and that the composition of the secondary biominerals produced would be correlated with the chemical and mineralogical composition of the original mineral resource.

Results

SEM images of Nkamouna laterite fragments following 14 days incubation with *A. niger* showed extensive crusts of shard-like biominerals (Fig. 1C and D). Control EDXA spectra showed peaks for Mn, O and Al, with smaller peaks also evident for C, Co, Ni and Fe (Fig. 2A). The EDXA spectra obtained for the biomineral crust reported Mn, Co and Ni as before, although Fe and Al peaks were absent, and an additional Mg peak was present. Additionally, the C peak was increased relative to the uninoculated control (Fig. 2B).

Table 1 summarizes pH, tolerance index and growth rate data for *A. niger* grown on MEA amended with 0.2% (w/v) Nkamouna laterite or synthetic Co-birnessite. The pH under *A. niger* biomass grown on laterite-amended media was pH 4.09, which is markedly higher than the pH 2.85 resulting on unamended, *A. niger* inoculated MEA. The pH value for uninoculated laterite-amended media was pH 5.92 after 14 days, while that of uninoculated MEA was pH 5.31. The tolerance index for *A. niger* on laterite-amended MEA was 97.7%, showing there was little decrease in biomass yield compared with *A. niger* grown on MEA. The growth rate ratio (R_m:R_c) was 1.42, which showed that the rate of colony expansion on laterite-amended MEA was markedly higher than that of the control. On synthetic Co-birnessite amended media, the average pH under the biomass was pH 2.17,

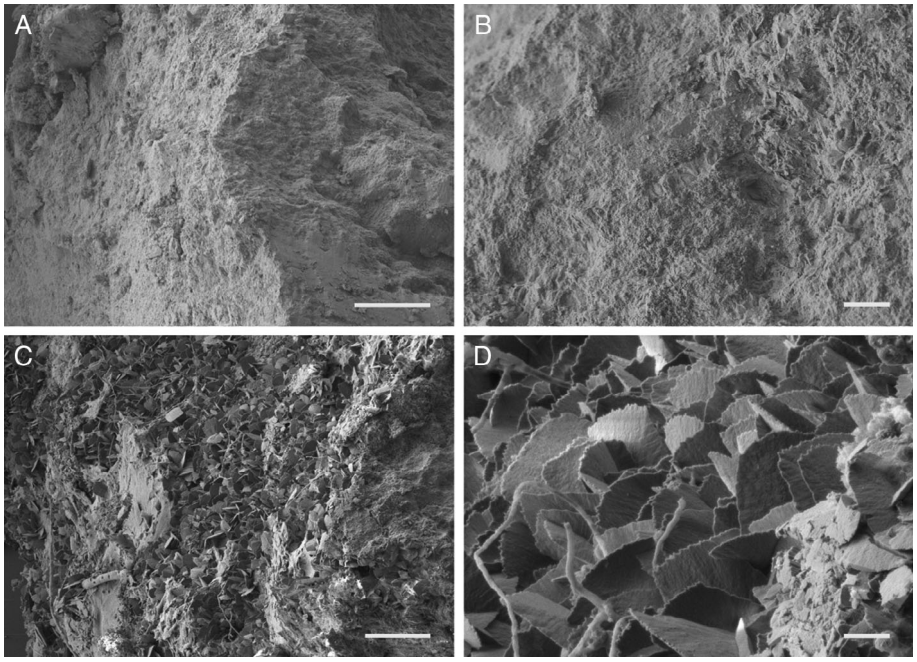

Fig 1. Biomineral formation on Nkamouna laterite fragments following incubation with *A. niger*. The SEM images show the formation of biomineral crusts on the Nkamouna laterite fragments following 2 weeks incubation at 25°C in the dark. (A, B) the surface of a fragment taken from an uninoculated control, (C, D) biomineral crust formation on fragments incubated with *A. niger*. Images were obtained using a JEOL SM-7400F field emission scanning electron microscope at an accelerating voltage of 5 keV. Images are representative of several examinations. Scale bars represent (A, C) 100 μm, (B, D) 10 μm.

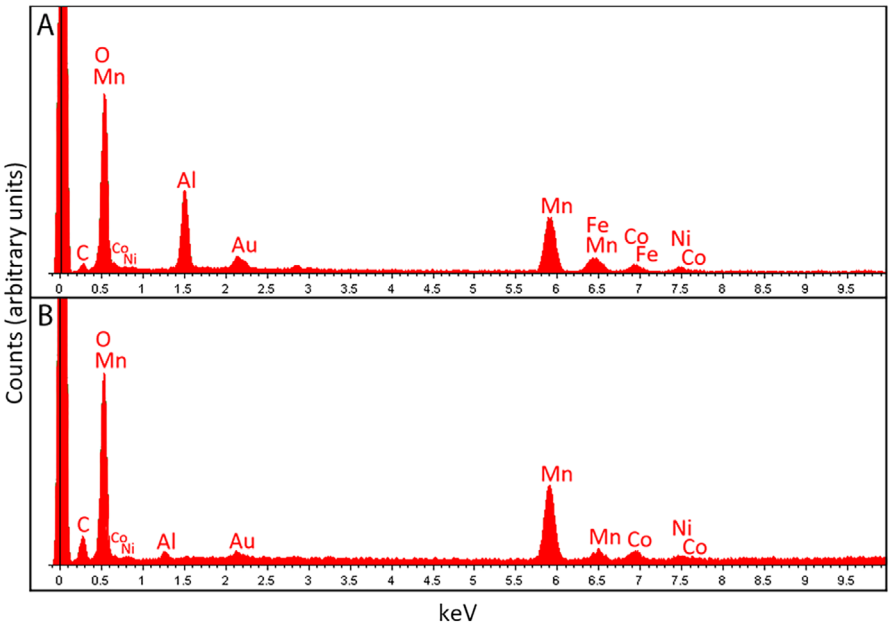

Fig 2. Elemental composition of biominerals formed on Nkamouna laterite fragments following incubation with *A. niger*. EDXA spectra obtained from (A) uninoculated control fragments of Nkamouna laterite recovered from uninoculated plates, (B) biomineral crust observed on Nkamouna laterite fragments recovered from plates following 14 days of incubation with *A. niger* at 25°C. The spectra shown are typical of several determinations. EDXA was carried out using a JEOL SM-7400F field emission scanning electron microscope at an accelerating voltage of 20 keV. [Color figure can be viewed at wileyonlinelibrary.com]

Table 1. Partial elemental composition of Nkamouna laterite and synthetic Co-birnessite as determined by XRF.

Element	Nkamouna Laterite (%)	Synthetic Co-birnessite (%)
MnO	30.91	73.41
Fe_2O_3	27.56	—
Al_2O_3	16.24	—
Co	5.04	7.74
SiO_2	3.90	—
Ni	2.87	—
Ba	0.78	—
Cr	0.50	—
MgO	0.24	—
K_2O	0.22	4.48
Ce	0.19	—
Cu	0.14	—
Zn	0.10	—
Pb	0.08	—
Na_2O	0.05	—
TiO_2	0.04	—
CaO	0.04	—
Cl	0.03	—

Note: Elements are expressed as oxides unless reported otherwise. Any elements detected by XRF that were not present in the solutions used to precipitate the Co-birnessite have been excluded. Analysis was carried out using a Philips 'Zetium' PW5400 sequential X-ray fluorescence spectrometer with a RhKα source (Malvern Panalytical, Malvern, UK). Samples were compacted under a load of 75 kN for 5 min, followed by 150 kN for 10 min before analysis.

compared with pH 2.26 for *A. niger* control growth on unamended MEA. Uninoculated Co-birnessite amended MEA reached pH 6.43 while uninoculated MEA plates were pH 5.32. The TI value was 94.1%, showing a small detrimental influence on biomass yield. The growth rate ratio (R_m:R_c) was 1.47, showing that *A. niger* colony expansion was considerably higher on Co-birnessite amended media compared with the control.

SEM images showing Nkamouna laterite powder debris following 14 days incubation with or without *A. niger* are shown in Fig. 3. Transformation was not total, with many laterite particles not showing morphological changes compared with the control mineral, although some biomineral formation was observed including the formation of shard-like crusts (Fig. 3B–D). These biomineral crusts displayed a morphology similar to that observed on the surface of Nkamouna laterite fragments, although they appeared poorly formed in comparison. Additional bipyramidal biominerals were also frequently observed (Fig. 3B and C). The uninoculated control EDXA spectra for mineral debris displayed peaks for Mn, O, Al and Co, with smaller peaks for C, Ni, Si and Fe (Fig. 4A). In comparison, biomineral crusts (Fig. 4B) showed increased peaks for Mn and Co, while the Al peak was reduced and Fe was not detected. EDXA of bipyramidal biomineral structures showed major peaks for calcium and smaller peaks for Mn, O and Al (Fig. 4C). XRPD analysis of the control Nkamouna laterite mineral debris showed patterns associated with lithiophorite [(Al, Li)]$MnO_2(OH)_2$] which was the dominant mineral phase, with additional patterns for cryptomelane ($K_{1\text{-}1.5}(Mn^{4+}$, $Mn^{3+})_8O_{16}$) (Fig. 5A). The transformed laterite also showed patterns for lithiophorite, with a reduced pattern for cryptomelane and an additional pattern for manganese oxalate dihydrate (Fig. 5B).

Figure 6 shows SEM images obtained for synthetic Co-birnessite following 14 days incubation with or without *A. niger*. Complete transformation was observed, with the fine, amorphous particles of Co-birnessite recovered from the uninoculated control (Fig. 6A) replaced with large

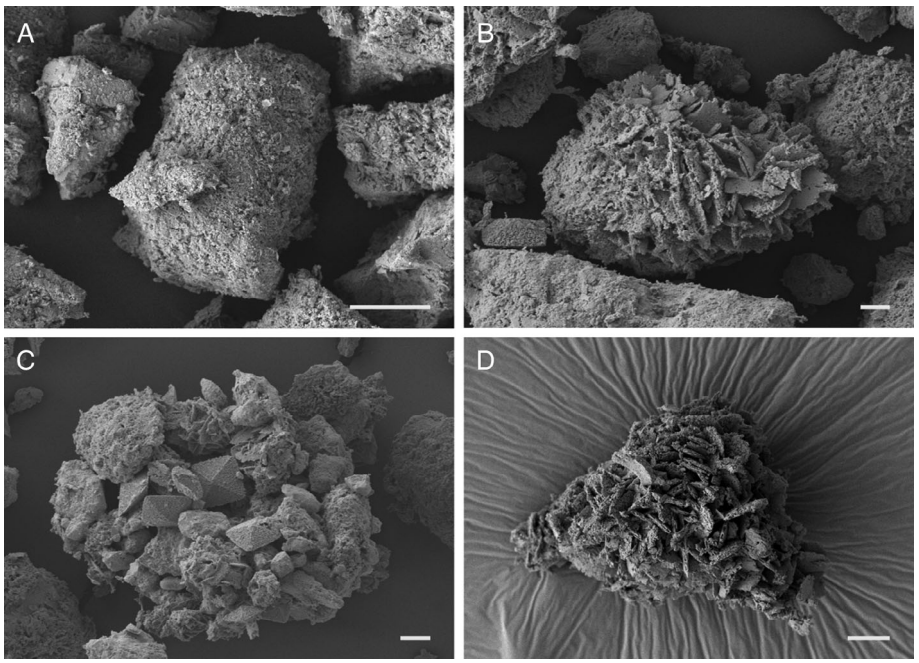

Fig 3. Nkamouna laterite powder transformation by *A. niger*. The SEM images show the extent of Nkamouna laterite powder transformation by *A. niger* following 2 weeks incubation at 25°C in the dark. (A) Laterite debris recovered from an uninoculated control, (B, C, D) mineral debris recovered from inoculated plates. Arrows indicate (mc) mineral crusts and (bp) bipyramidal secondary mineral structures. Images were obtained using a JEOL SM-7400F field emission scanning electron microscope at an accelerating voltage of 5 keV. Scale bars represent (A) 100 μm, (B, C, D) 10 μm.

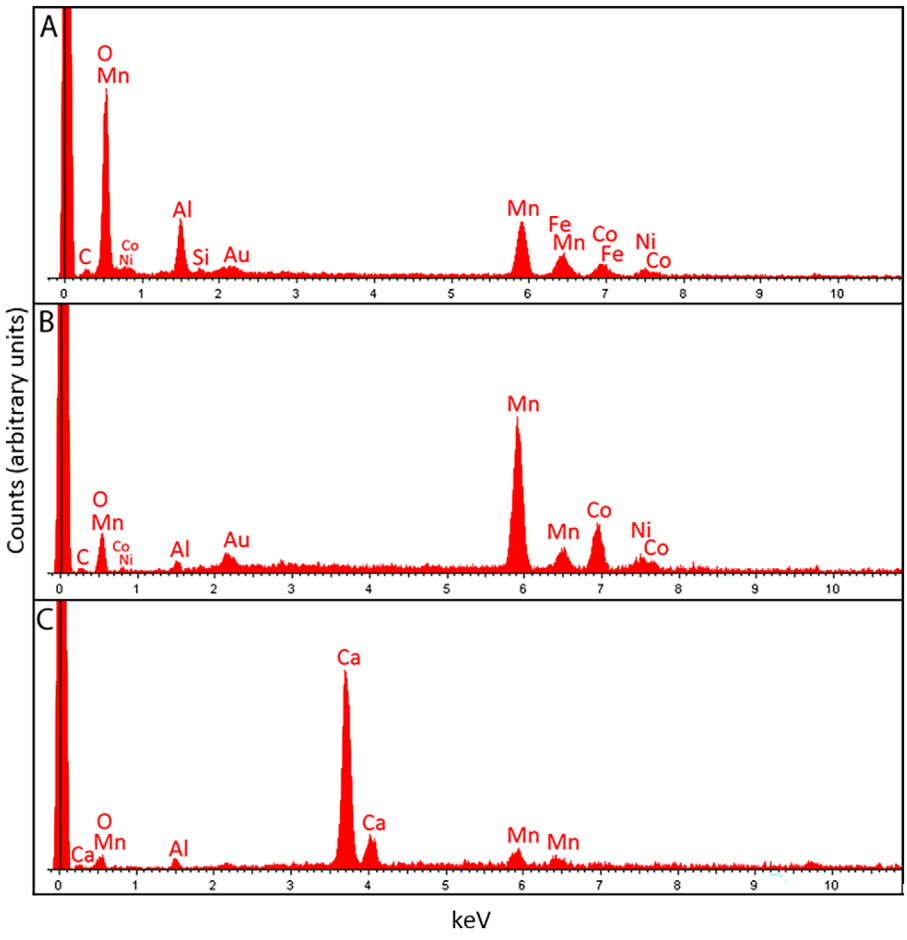

Fig 4. Elemental composition of Nkamouna laterite powder after incubation with *A. niger*. EDXA spectra obtained for (A) uninoculated control Nkamouna laterite powder recovered from uninoculated plates, (B) biomineral crusts and (C) bipyramidal structures in mineral debris recovered from laterite-amended plates inoculated with *A. niger*. The spectra shown are typical of several determinations. Analysis was carried out using a JEOL SM-7400F field emission scanning electron microscope at an accelerating voltage of 20 keV. [Color figure can be viewed at wileyonlinelibrary.com]

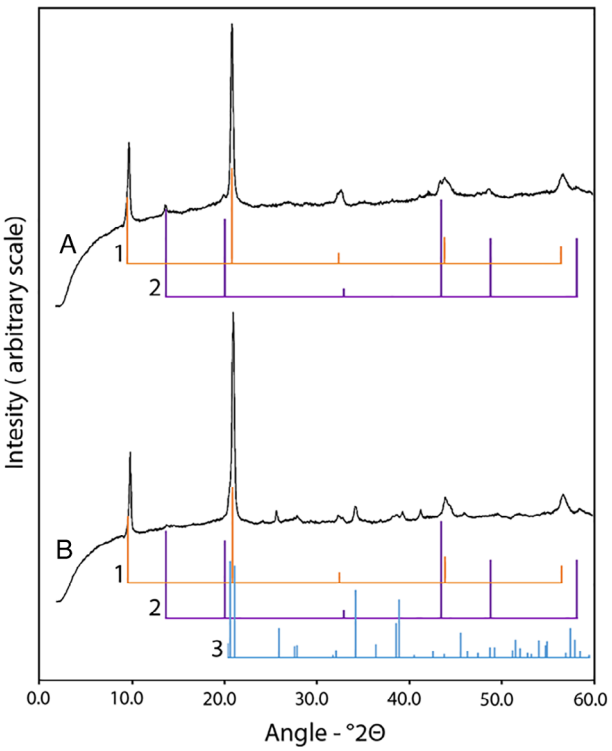

Fig 5. XRPD of transformed Nkamouna laterite powder. XRPD patterns for mineral debris recovered from MEA plates amended with 0.2% (w/v) Nkamouna laterite following 14 days incubation with *A. niger* are shown. (A) mineral debris recovered from an uninoculated control and (B) mineral debris recovered from a mineral-amended plate inoculated with *A. niger*. Patterns correspond to (1) lithiophorite ($(Al,Li)MnO_2(OH)_2$), (2) cryptomelane ($K_{1\text{-}1.5}(Mn^{4+}, Mn^{3+})_8O_{16}$) and (3) manganese oxalate dihydrate (lindbergite, $MnC_2O_4{\cdot}2H_2O$). Typical patterns are shown from several determinations. [Color figure can be viewed at wileyonlinelibrary.com]

rosette structures (Fig. 6B–D). These rosette structures were up to approximately 100 μm in diameter (Fig. 6D). The EDXA spectra obtained for the uninoculated control Co-birnessite material showed clear peaks for Mn, O, K and Co (Fig. 7A). The spectrum obtained from the transformed material (Fig. 7B) also showed peaks for Mn, O and Co, although K was not detected and there was an additional C peak compared with the control. Uninoculated control material showed XRD patterns for birnessite (Fig. 8A), while the transformed mineral debris showed patterns corresponding to manganese oxalate dihydrate (lindbergite, $MnC_2O_4{\cdot}2H_2O$) (Fig. 8B).

Discussion

A. niger was able to transform Nkamouna laterite in both fragmented and powder form in both cases resulting in the formation of shard-like biomineral surface crusts. On the Nkamouna fragments, the observed biominerals contained Mn, Co, Ni, Mg, C and O as major elements while Al and Fe were absent. Considering the Al content of lithiophorite, it can be concluded that this represents a clear transformation of the original Nkamouna material. XRPD analysis confirmed that this was a Mn oxalate phase containing lesser amounts of Co, Ni and Mg, all of which can readily precipitate as oxalates (Yang *et al*., 2020; Suyamud *et al*., 2020). As Al(III) and Fe(III) do not precipitate but form soluble oxalate complexes, it is likely that these elements were solubilized and removed. Furthermore, given the high sorptive capacity of Mn oxide minerals, it is also possible that Al(III) and Fe(III) were re-adsorbed onto the Nkamouna laterite as either aqueous or hydrolysed cations (Nicholson and Eley, 1997). The composition of biominerals encrusting Nkamouna laterite powder was also similar, showing a decrease in Al relative to the control, an absence of Fe, the presence of Mn, Co and Ni and the presence of Mn(II) oxalate dihydrate. It is unclear whether lithiophorite or cryptomelane were equally susceptible to attack by oxalic acid although, given the absence or decrease in Al content following transformation, it can be assumed that lithiophorite was certainly affected. This is particularly significant as lithiophorite is known to host particularly high Co concentrations (Post, 1999) and is the principle Co host phase in Nkamouna laterite (Yongue-Fouateu *et al*., 2006; Dzemua *et al*., 2013). The presence of bipyramidal Ca-bearing biominerals characteristic of Ca oxalate dihydrate (weddellite) further illustrated the role of oxalate (Gadd *et al*., 2014). Taken together, these results demonstrate that an oxalate-producing fungus can effect the transformation of Mn oxides in a laterite ore, and that hosted Co, Ni and Mg can be incorporated into the resulting Mn(II) oxalate to form a mixed oxalate biomineral phase. Synthetic Co-birnessite was also transformed by *A. niger*, with total solubilization of the original material observed. SEM revealed large rosette biomineral structures, similar to those observed following oceanic manganese nodule colonization by *A niger* (Ferrier *et al*., 2019) Moreover, EDXA showed the absence of K and the presence of C, O, Mn and Co, confirming solubilization of the synthetic birnessite, release of K, and precipitation of a Co-bearing Mn oxalate, the latter being confirmed by XRD. As Mn is hosted as Mn(III,IV) in lithophorite, cryptomelane and birnessite, oxalate excretion involves reduction to Mn(II) (Ehrlich and Newman, 2009; Wei *et al*., 2012). Moreover, given that Co is structurally incorporated into MnO_6 layers as Co(III), it is reasonable to suggest that reduction to Co(II) by oxalate occurred prior to oxalate precipitation in both the natural and synthetic material (Manceau *et al*., 1997). The increased pH of mineral-amended media (Table 2) and the buffering effect of manganese oxides are likely to be responsible for the increased growth ratio (R_m:R_C) on this substrate since *A. niger* exhibits stable growth between pH 2 and pH 8 (Andersen *et al*., 2009).

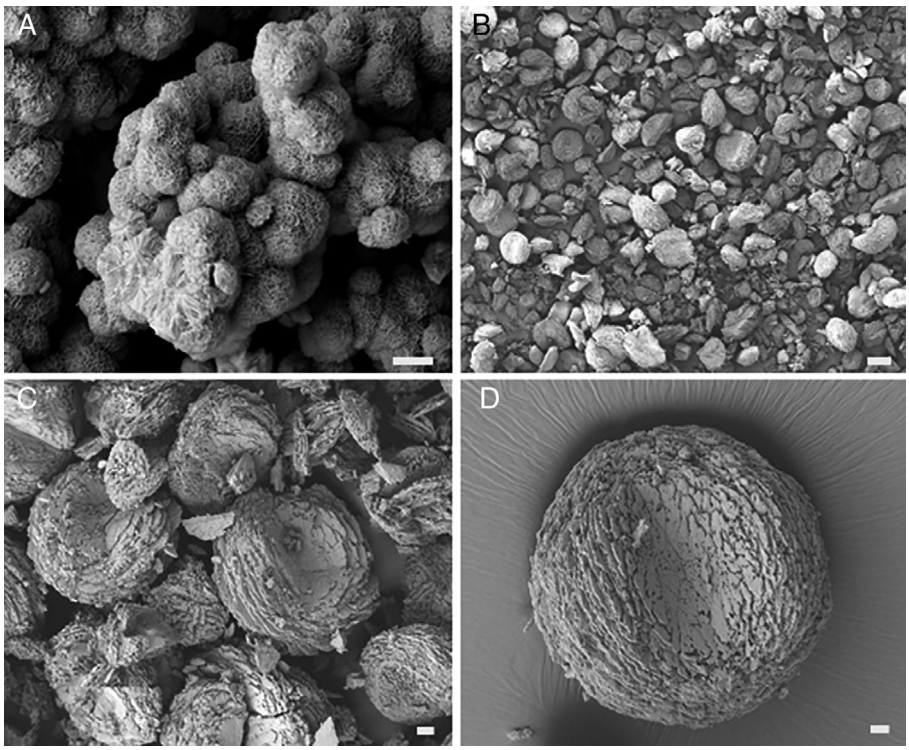

Fig 6. Synthetic Co-birnessite transformation following incubation with *A. niger*. The SEM images show the extent of synthetic Co-birnessite transformation by *A. niger* following 2 weeks incubation at 25°C in the dark. (A) synthetic Co-birnessite debris recovered from an uninoculated control, (B, C, D) mineral debris recovered from inoculated plates. Images were obtained using a JEOL SM-7400F field emission scanning electron microscope operating at an accelerating voltage of 5 keV. Scale bars represent (A) 1 μm, (B) 100 μm, (C, D) 10 μm. Typical images are shown from several examinations.

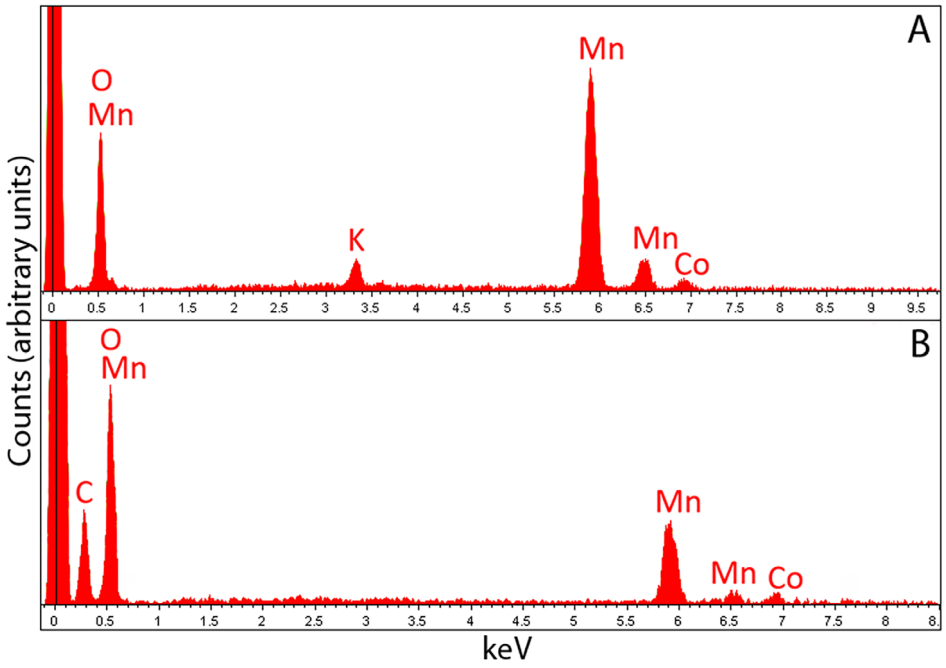

Fig 7. Elemental composition of synthetic Co-birnessite following incubation with *A. niger*. The EDXA spectra shown were obtained from (A) control synthetic Co-birnessite recovered from uninoculated plates, (B) transformed mineral debris recovered from plates incubated with *A. niger* for 14 days at 25°C in the dark.. Spectra shown are typical of several determinations. Analysis was carried out using a JEOL SM-7400F field emission scanning electron microscope at an accelerating voltage of 20 keV. [Color figure can be viewed at wileyonlinelibrary.com]

Our results demonstrate that transformation of Mn oxide minerals by mycogenic oxalate results in the mobilization and immobilization of secondary metal and non-metal components based primarily on ionic species. Divalent metals that readily form insoluble oxalates can be co-hosted in mixed oxalate biomineral phases, while mono- and trivalent cations are solubilized, presumably as free cations and/or soluble oxalate complexes (Gadd, 1999; Gadd *et al*., 2014; Verma *et al*., 2019). In anaerobic conditions, the mobility of metals hosted in Mn oxides has been shown to be influenced by the action of Mn(IV)- and Fe(III)-reducing prokaryotes (Newsome

Table 2. The media pH, tolerance indices and growth rates of *A. niger* on mineral-amended MEA.

	pH					
	A. niger + mineral	*A. niger* control − mineral	Abiotic control + mineral	Abiotic control − mineral	Tolerance Index (TI)	Growth (R_m:R_c)
Nkamouna laterite	4.09 ± 0.29$^{(5)}$	2.85 ± 0.06$^{(4)}$	5.92 ± 0.04$^{(3)}$	5.31 ± 0.02$^{(3)}$	97.7	1.42
Synthetic Co-birnessite	2.17 ± 0.03$^{(6)}$	2.26 ± 0.02$^{(3)}$	6.43 ± 0.04$^{(2)}$	5.32 ± 0.02$^{(3)}$	94.1	1.47

Note: The pH of media under biomass, tolerance index (TI) after 14 days incubation, and growth rate ratios of *A. niger* on MEA media without or amended with 0.2% (w/v) Nkamouna laterite or synthetic Co-birnessite are shown. Data are averages or were calculated from separate averages. TI is a ratio, expressed as %, of the dry weight of biomass yield on mineral-amended media to that obtained on mineral-free MEA controls, where a TI of 100% indicates a biomass yield equal to that of the control. Growth rates are expressed as a ratio of the average daily growth rate between days 2–5 for *A. niger* grown on Nkamouna laterite amended MEA (R_m) to that of control growth on MEA (R_c): a R_m:R_c of 1.0 indicates that the rate of colony expansion in mineral-amended medium was the same as the control. Average control biomass yields were: 306 (SD ± 0.01) mg (Nkamouna), 275 (SD ± 0.001) mg (Co-birnessite). Average control growth rates between days 2–5 were: 9.94 (SD ± 0.20) mm/day (Nkamouna), 8.67 (SD ± 0.31) mm/day (Co-birnessite). Standard deviations are shown (±) and superscript numbers denote the number of replicates. Incubations were carried out at 25°C in the dark for 14 days.

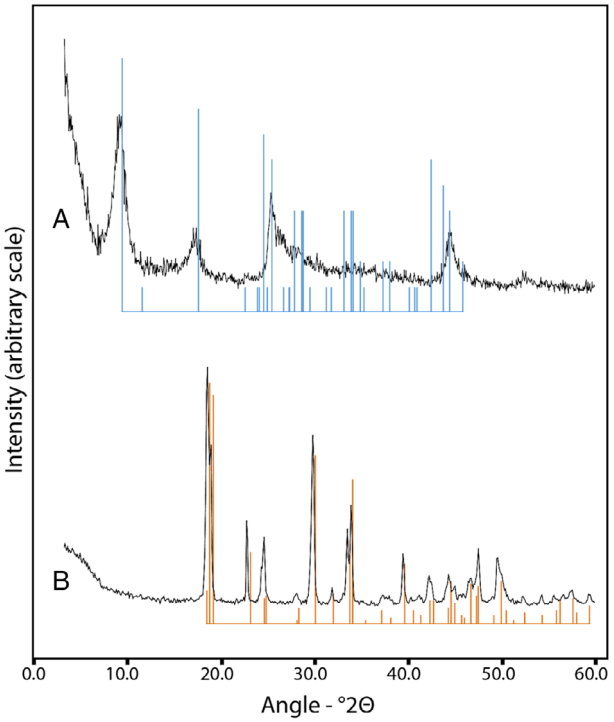

Fig 8. XRPD of transformed Nkamouna laterite powder. XRPD spectra of mineral debris recovered from (A) uninoculated control synthetic Co-birnessite plates and (B) mineral-amended plates inoculated with *A. niger* following 14 days incubation at 25°C in the dark. Replicates were pooled and a subsample analysed. Blue patterns correspond to birnessite, orange patterns correspond to manganese oxalate dihydrate (lindbergite, $MnC_2O_4{\cdot}2H_2O$). Typical patterns are shown from several determinations. [Color figure can be viewed at wileyonlinelibrary.com]

et al., 2020). The data presented here clearly demonstrate that aerobic oxalate producing fungi, which are ubiquitous in terrestrial environments, can act in an opposing manner to extract and immobilize metals as insoluble oxalates. Moreover, the presence of fungal genera capable of oxalate excretion, e.g. *Penicillium* spp., were confirmed in a range of lateritic deposits shown to also host Mn(IV)- and Fe(III)-reducing prokaryotes and containing Co-bearing Mn oxides (Newsome *et al*., 2020). It is interesting to speculate that the speciation of Co in terrestrial Mn oxide deposits could be influenced by both Mn(IV) and Fe(III) reducing prokaryotes and organic acid producing fungi depending on environmental factors such as oxygen and nutrient availability.

Experimental procedures

Organism, media and growth conditions

Experiments were conducted using *A. niger* ATCC 1015 which was maintained on 90 mm diameter malt extract agar (MEA) plates (LabM, Bury, UK) at 25°C in the dark. Media for powder transformation experiments was prepared by adding sterile mineral powder to molten MEA at ~60°C to a concentration of 0.2% (w/v) and mixing before adding ~25 cm^3 of the resulting media to 90 mm diameter Petri dishes. For Nkamouna fragment transformation, sterile fragments were set into wells in MEA plates which were prepared by melting the agar using forceps that were heated briefly over a Bunsen burner. All mineral-amended MEA plates were inoculated with one 5 mm diameter plug of *A. niger* taken from the edge of a colony actively growing on MEA using a sterile cork borer, and incubated for 14 days. Growth measurements on mineral powder amended MEA plates were taken by measuring two bisecting colony diameters at appropriate time intervals.

Minerals

Nkamouna laterite was originally obtained directly from Nkamouna, Cameroon and kindly provided by Dr

D.S. Mulroy (Department of Earth and Environmental Sciences, University of Manchester, UK) and broken down to fragmented and powder forms using a mortar and pestle. Synthetic Co-bearing birnessite was prepared according to McKendry *et al*. (2018) as follows: 50 ml of 1.1 M $CoCl_2{\cdot}6H_2O$ was added to 250 ml of a 0.2 M aqueous solution of $KMnO_4$ heated to 80°C with stirring at 360 rpm, followed by slow, dropwise addition of 50 ml 3 M HCl. The resulting solution was left for a further 30 min before reducing the temperature to 50°C for a further 15 h. The precipitate was then recovered by centrifuging (3913 g × 20 min) before removing the supernatant and resuspending the pellet in Milli-Q water. The washing process was repeated three times before drying the precipitate in a desiccator for at least 7 days to constant weight. Once dry, the Co-birnessite precipitate was added to 200 ml 0.1 HNO_3 and shaken at 125 rpm at 25°C for 2 days in order to exchange interlayer K^+ for H^+, as described by Peng *et al*. (2017). The precipitate was then recovered and dried as described above. Minerals were sieved to a particle diameter of <90 μm using soil sieves (Endecotts, London, UK) and sterilized in an oven at 105°C for at least 24 h prior to experimentation.

pH measurements

Following 14 days incubation on solid media, fungal biomass was carefully removed using a scalpel and the pH of the agar underneath the mycelium measured using a flat-tipped pH electrode (VWR International Ltd, Lutterworth, UK), which enables good contact with the agar surface, and an Orion 920+ pH meter (ThermoFisher Scientific, Loughborough, UK).

Mineral recovery

Following pH measurement, minerals were recovered from the agar by gently homogenizing in Milli-Q water heated to approximately 70°C in a glass crystallizing dish. The mineral debris were allowed to settle and the fluid removed, this process being repeated twice. Finally, mineral debris was dried in a desiccator for at least 48 h.

X-ray fluorescence (XRF)

Partial elemental composition of the original mineral samples was determined using a Philips 'Zetium' PW5400 sequential X-ray fluorescence spectrometer filtered with a RhKα source (Malvern Panalytical, Malvern, UK). Samples were compacted under a load of 75 kN for 5 min, followed by 150 kN for 10 min before analysis. The results are expressed as oxides unless reported otherwise.

Scanning electron microscopy (SEM) and energy dispersive X-ray analysis (EDXA)

Transformed mineral samples were mounted on 25 mm × 5 mm aluminium electron microscopy stubs using double-sided adhesive carbon tape before coating with gold and palladium to a thickness of 25 nm using a Cressington 208HR sputter coater (Cressington Scientific Instruments, Watford, UK). SEM and EDXA examination was conducted using a field emission scanning electron microscope (JEOL SM-7400F), operating at an accelerating voltage of 5 kV for imaging and 20 kV for EDXA. Any adjustments to contrast and/or brightness made after the image was taken were carried out using Adobe Photoshop CS5.1 and were applied equally to the whole image.

X-ray diffraction (XRD)/X-ray powder diffraction (XRPD)

Transformed Nkamouna samples were analysed using XRPD and transformed Co-birnessite samples were analysed using XRD. XRPD analysis was conducted using an Enraf-Nonius FR590 powder diffraction system (Enraf-Nonius, Rotterdam, Netherlands). Samples were prepared by grinding using a mortar and pestle before applying to a quartz substrate via an acetone smear. Diffraction patterns were then recorded from 0 to 80° 2-theta using an INEL 120° curved position sensitive detector, with Co K-alpha radiation. The samples were continuously spun in the plane of the sample surface for a 2 h data collection period. XRD analysis was conducted using a Siemens D5000 powder X-ray diffractometer (Siemens Healthineers, Henkestraße 127, 91052 Erlangen, Germany). Samples were ground to a fine powder using a mortar and pestle before applying to PVC slides. Diffraction patterns were recorded using angular increments of 0.1° 2-theta, from 3 to 60° 2-theta, at a rate of 1° 2-theta/min. A Cu-Kα source was used, operating at 40 mA and 40 kV, with a scintillation detector.

Acknowledgements

G.M.G. gratefully acknowledges funding for this research from the Natural Environment Research Council (NERC) (NE/M011275/1 (COG^3 – the geology, geometallurgy and geomicrobiology of cobalt resources leading to new product streams) and further support of the Geomcrobiology Group from NERC grant NE/M010910/1 (TeaSe). J.F. gratefully acknowledges receipt of a NERC PhD studentship as part of the COG^3 award. Dr. Yongchan Fan (School of Science and Engineering, University of Dundee) for assistance with SEM and EDXA.

References

Andersen, M.R., Lehmann, L., and Nielsen, J. (2009) Systemic analysis of the response of *Aspergillus Niger* to ambient pH. *Genome Biol* **10**: R47.

Arias, N.P., Becerra, M.E., and Giraldo, O. (2019) Structural and electrical studies for birnessite-type materials synthesised by solid-state reactions. *Nanomaterials* **9**: 1156.

Burford, E., Hillier, S., and Gadd, G.M. (2006) Biomineralization of fungal hyphae with calcite ($CaCO_3$) and calcium oxalate mono- and dihydrate in carboniferous limestone microcosms. *Geomicrobiol J* **23**: 599–611.

Burford, E.P., Fomina, M., and Gadd, G.M. (2003) Fungal involvement in bioweathering and biotransformation of rocks and minerals. *Mineral Mag* **67**: 1127–1155.

Ceci, A., Kierans, M., Hillier, S., Persiani, A.M., and Gadd, G.M. (2015) Fungal bioweathering of mimetite and a general geomycological model for lead apatite mineral biotransformations. *Appl Environ Microbiol* **81**: 4955–4964.

Cheney, M.A., Jose, R., Banerjee, A., Bhowmik, P.K., Qian, S., and Okoh, J.M. (2009) Synthesis and characterization of birnessite and cryptomelane nanostructures in presence of hoffmeister anions. *J Nanomater* **2009**: 940462.

Chukhrov, F.V., Gorshkov, A.I., Vitovskaya, I.V., Drits, V.A., and Sivstov, A.V. (1982) On the nature of co-Ni asbolane; a component of some supergene ores. In *Ore Genesis the State of the Art. Special Publication No. 2 of the Society for Geology Applied to Mineral Deposits*, Amstuz, G.C., El Goresy, A., Frnzel, G., Kluth, C., Moh, G., Wauschkuhn, A., and Zimmerman, R.A. (eds). Berlin, Heidelberg, New York: Springer-Verlag.

Dzemua, G.L., Gleeson, S.A., and Schofield, P.F. (2013) Mineralogical characterization of the Nkamouna co-Mn laterite ore, Southeast Cameroon. *Miner Deposita* **48**: 155–177.

Dzemua, G.L., Mees, F., Stoops, G., and Ranst, E.V. (2011) Micromorphology, mineralogy and geochemistry of lateritic weathering over serpentinite in south-East Cameroon. *J Afr Earth Sci* **20**: 38–48.

Ehrlich, H.L., and Newman, D.K. (2009) *Geomicrobiology*, 5th ed. Boca Raton, FL: CRC Press/Taylor & Francis.

Ferrier, J., Yang, Y., Csetenyi, L., and Gadd, G.M. (2019) Colonization, penetration and transformation of manganese oxide nodules by *Aspergillus Niger*. *Environ Microbiol* **21**: 1821–1832.

Fomina, M., Alexander, I.J., Hillier, S., and Gadd, G.M. (2004) Zinc phosphate and pyromorphite solubilization by soil plant-symbiotic fungi. *Geomicrobiol J* **21**: 351–366.

Fomina, M., Charnock, J.M., Hillier, S., Alvarez, R., and Gadd, G.M. (2007) Fungal transformations of uranium oxides. *Environ Microbiol* **9**: 1696–1710.

Gadd, G.M. (1999) Fungal production of citric and oxalic acid: importance in metal speciation, physiology and biogeochemical processes. *Adv Microb Physiol* **41**: 47–92.

Gadd, G.M. (2007) Geomycology: biogeochemical transformations of rocks, minerals, metals and radionuclides by fungi, bioweathering and bioremediation. *Mycol Res* **111**: 3–49.

Gadd, G.M. (2010) Metals, minerals and microbes: geomicrobiology and bioremediation. *Microbiology* **156**: 609–643.

Gadd, G.M., Bahri-Esfahani, J., Li, Q., Rhee, Y.J., Fomina, M., and Liang, X. (2014) Oxalate production by fungi: significance in geomycology, biodeterioration and bioremediation. *Fungal Biol Rev* **28**: 36–55.

Händel, M., Rennert, T., and Tosche, K.U. (2013) A simple method to synthesize birnessite at ambient pressure and temperature. *Geoderma* **193-194**: 117–121.

Hein, J.R., Mizell, K., Koschinsky, A., and Conrad, T.A. (2013) Deep-ocean mineral deposits as a source of critical metals for high- and green-technology applications: comparison with land-based resources. *Ore Geol Rev* **51**: 1–14.

Jokic, A., Frenkel, A.I., Vairavamurthy, M.A., and Huang, P. M. (2001) Birnessite catalysis of the Maillard reaction: its significance in natural humification. *Geophys Res Lett* **28**: 3899–3902.

Kang, X., Csetenyi, L., and Gadd, G.M. (2019) Biotransformation of lanthanum by *Aspergillus Niger*. *Appl Microbiol Biotechnol* **103**: 991–993.

Kang, X., Csetenyi, L., and Gadd, G.M. (2020) Monazite transformation into Ce- and La-containing oxalates by *Aspergillus Niger*. *Environ Microbiol* **22**: 1635–1648.

Kang, X., Csetenyi, L., and Gadd, G.M. (2021) Colonization and bioweathering of monazite by *Aspergillus Niger*: solubilization and precipitation of rare earth elements. *Environ Microbiol*. https://sfamjournals.onlinelibrary.wiley.com/doi/epdf/10.1111/1462-2920.15402

Kuhn, T., Wgorzewski, C., Rühleman, C., and Vink, A. (2017) Composition, formation and occurrence of polymetallic nodules. In *Deep Sea Mining: Resource Potential, Technical and Environmental Considerations*, Sharma, R. (ed). New York, NY: Springer International Publishing, pp. 23–63.

Legutko, P., Pęza, J., Rossi, A.V., Marzec, M., Jakubek, T., and Kozieł. (2019) Elucidation of unexpectedly weak catalytic effect of doping with cobalt of the cryptomelane and birnessite systems active in soot combustion. *Top Catal* **62**: 599–610.

Liang, X., Hillier, S., Pendlowski, H., Gray, N., Ceci, A., and Gadd, G.M. (2015) Uranium phosphate biomineralization by fungi. *Environ Microbiol* **17**: 2064–2075.

Lovley, D.R. (1991) Dissimilatory Fe(III) and Mn(IV) reduction. *Microbiol Rev* **55**: 259–287.

Lovley, D.R., Holmes, D.E., and Nevin, K.P. (2004) Dissimilatory Fe(III) and Mn(IV) reduction. *Adv Microb Physiol* **49**: 219–286.

Lucht, K.P., and Medoza-Cortex, J.L. (2015) Birnessite: a layered manganese oxide to capture sunlight for water-splitting catalysis. *J Phys Chem* **119**: 22838–22846.

Manceau, A., Drits, V.A., Silvester, E., Bartoli, C., and Lanson, B. (1997) Structural mechanism of Co^{2+} oxidation by the phyllomanganate buserite. *Am Mineral* **82**: 1150–1175.

McKendry, I.G., Thenuwara, A.C., Shumlas, S.L., Peng, H., Aulin, Y.V., Chinnam, P.R., *et al*. (2018) Systematic doping of cobalt into layered manganese oxide sheets substantially enhances water oxidation catalysis. *Inorg Chem* **57**: 557–564.

Mendes, G.d.O., Bahri-Esfahani, J., Csetenyi, L., Hillier, S., George, T.S., and Gadd, G.M. (2020) Chemical and physical mechanisms of fungal bioweathering of rock phosphate. *Geomicrobiol J*, https://doi.org/10.1080/01490451.2020.1863525.

Milová-Žiaková, B., Urík, M., Boriová, K., Bujdoš, M., Mikušová, P., Takáčová, A., and Matúš. (2016) Fungal solubilization of manganese oxide and its significance for antimony mobility. *Int Biodeterior Biodegrad* **114**: 157–163.

Miyata, N., Tani, Y., Iwahori, K., and Soma, M. (2004) Enzymatic formation of manganese oxides by an *Acremonium*-like hyphomycete fungus, strain KR21-2. *FEMS Microbiol Ecol* **47**: 101–109.

Miyata, N., Maruo, K., Tani, Y., Tsuno, H., Seyama, H., Soma, M., and Iwahori, K. (2006a) Production of biogenic manganese oxides by anamorphic ascomycete fungi isolated from streambed pebbles. *Geomicrobiol J* **23**: 63–73.

Miyata, N., Tani, T., Maruo, K., Tsuno, H., Sakata, M., and Iwahori, K. (2006b) Manganese(IV) oxide production by *Acremonium* sp. strain KR21-2 and extracellular Mn(II) oxidase activity. *Appl Environ Microbiol* **72**: 6467–6473.

Newsome, L., Arguedas, A.S., Coker, V.S., Boothman, C., and Lloyd, J.R. (2020) Manganese and cobalt redox cycling in laterites: biogeochemical and bioprocessing implications. *Chem Geol* **531**: 119330.

Nicholson, K., and Eley, M. (1997) Geochemistry of manganese oxides: metal adsorption in freshwater and marine environments. In *Manganese Mineralization: Geochemistry and Mineralogy of Terrestrial and Marine Deposits*, Vol. **119**, Nicholson, K., Hein, J.R., Bühn, B., and Dasgupta, S. (eds). London, UK: Geological Society Special Publication, pp. 309–326.

Peng, H., McKendry, I.G., Ding, R., Thenuwara, A.C., Kang, Q., Shumlas, S.L., *et al*. (2017) Redox properties of birnessite from a defect perspective. *Proc Natl Acad Sci U S A* **114**: 9523–9528.

Petavratzi, E., Gunn, G., & Kresse, C. (2019). Commodity review: Cobalt. *British Geological Survey*. https://www.researchgate.net/publication/337604314_BGS_COMMODITY_REVIEW_Cobalt

Post, J.E. (1999) Manganese oxide minerals: crystal structures and economic and environmental significance. *Proc Natl Acad Sci U S A* **96**: 3447–3454.

Rhee, Y.J., Hillier, S., and Gadd, G.M. (2012) Lead transformation to pyromorphite by fungi. *Curr Biol* **22**: 237–241.

Santelli, C.M., Webb, S.M., Dohnalkova, A.C., and Hansel, C.M. (2011) Diversity of Mn oxides produced by Mn(II)-oxidizing fungi. *Geochim Cosmochim Acta* **75**: 2762–2776.

Sayer, J.A., and Gadd, G.M. (2001) Binding of cobalt and zinc by organic acids and culture filtrates of *Aspergillus Niger* grown in the absence of presence of insoluble cobalt or zinc phosphate. *Mycol Res* **105**: 1261–1267.

Suyamud, B., Ferrier, J., Csetenyi, L., Inthorn, D., and Gadd, G.M. (2020) Biotransformation of struvite by *Aspergillus Niger*: phosphate release and magnesium biomineralization as glushinskite. *Environ Microbiol* **22**: 1588–1602.

Tebo, B.M., Bargar, J.R., Clement, B.G., Dick, G.J., Murray, K.J., Parker, D., *et al*. (2004) Biogenic manganese oxides: properties and mechanisms of formation. *Annu Rev Earth Planet Sci* **32**: 287–328.

Toner, B., and Sposito, G. (2005) Reductive dissolution of biogenic manganese oxides in the presence of hydrated biofilm. *Geomicrobiol J* **22**: 171–180.

Verma, A., Kore, R., Corbin, D., and Shiflett, M.B. (2019) Metal recovery using oxalate chemistry: a technical review. *Ind Eng Chem Res* **58**: 15381–15393.

Wang, N., Liang, C., Du, L., and Cui, H. (2013) Arsenite sorption and oxidation by synthetic birnesste. *J Water Supply Res Technol* **64**: 245–253.

Wei, Z., Hillier, S., and Gadd, G.M. (2012) Biotransformation of manganese oxides by fungi: solubilization and production of manganese oxalate biominerals. *Environ Microbiol* **14**: 1744–1753.

Wei, Z., Liang, X., Pendlowski, H., Hillier, S., Suntornvongsagul, K., Sihanonth, P., and Gadd, G.M. (2013) Fungal biotransformation of zinc, silicate and sulfide mineral ores. *Environ Microbiol* **15**: 2173–2186.

Yadav, G.G., Gallaway, J.W., Turney, D.E., Nyce, M., Huang, J., Wei, X., and Banerjee, S. (2017) Regenerable Cu-intercalated MnO_2 layered cathode for highly cyclable energy dense batteries. *Nat Commun* **8**: 14424.

Yang, Y., Ferrier, J., Csetenyi, L., and Gadd, G.M. (2019) Direct and indirect bioleaching of cobalt from low grade laterite and pyritic ores by *Aspergillus Niger*. *Geomicrobiol J* **36**: 940–949.

Yang, Y., Song, W., Ferrier, J., Liu, F., Csetenyi, L., and Gadd, G.M. (2020) Biorecovery of cobalt and nickel using biomass-free culture supernatants from *Aspergillus Niger*. *Appl Microbiol Biotechnol* **104**: 417–425.

Yongue-Fouateu, R., Ghogomu, R.T., Penaye, J., Ekodeck, G.E., Stendal, H., and Colin, F. (2006) Nickel and cobalt distribution in the laterites of the Lomié region, south-East Cameroon. *J Afr Earth Sci* **45**: 33–47.